


Article

Investigation on the Compressibility Factor of Hydrogen-Doped Natural Gas Using GERG-2008 Equation of State

Ji-Chao Li ^{1,†} , Yong Fan ^{2,†}, Dan Pang ³, Tong Wu ², Ying Zhang ^{1,*} and Ke Zhou ^{1,*}¹ School of Mechanical Engineering, Jining University, Qufu 273155, China; lijichao@jnxu.edu.cn² School of Transportation, Ludong University, Yantai 264025, China; 19861064715@163.com (Y.F.); wutong3224599684@163.com (T.W.)³ Liaoshen Industry Group Corporation Limited, Shenyang 110045, China; pangdan2024@163.com

* Correspondence: zhangyingcad@126.com (Y.Z.); zhouke@jnxu.edu.cn (K.Z.)

† These authors contributed equally to this work.

Abstract: The primary methods for hydrogen transportation include gaseous storage and transport, liquid hydrogen storage, and transport via organic liquid carriers. Among these, pipeline transportation offers the lowest cost and the greatest potential for large-scale, long-distance transport. Although the construction and operation costs of dedicated hydrogen pipelines are relatively high, blending hydrogen into existing natural gas networks presents a viable alternative. This approach allows hydrogen to be transported to the end-users, where it can be either separated for use or directly combusted, thereby reducing hydrogen transport costs. This study, based on the GERG-2008 equation of state, conducts experimental tests on the compressibility factor of hydrogen-doped natural gas mixtures across a temperature range of $-10\text{ }^{\circ}\text{C}$ to $110\text{ }^{\circ}\text{C}$ and a pressure range of 2 to 12 MPa, with hydrogen blending ratios of 5%, 10%, 20%, 30%, and 40%. The results indicate that the hydrogen blending ratio, temperature, and pressure significantly affect the compressibility factor, particularly under low-temperature and high-pressure conditions, where an increase in the hydrogen blending ratio leads to a notable rise in the compressibility factor. These findings have substantial implications for the practical design of hydrogen-enriched natural gas pipelines, as changes in the compressibility factor directly impact pipeline operational parameters, compressor characteristics, and other system performance aspects. Specifically, the introduction of hydrogen alters the compressibility factor of the transported medium, thereby affecting the pipeline's flowability and compressibility, which are crucial for optimizing and applying the performance of hydrogen-enriched natural gas in transportation channels. The research outcomes provide valuable insights for understanding combustion reactions, adjusting pipeline operational parameters, and compressor performance characteristics, facilitating more precise decision-making in the design and operation of hydrogen-enriched natural gas pipelines.

Keywords: compression factor; natural gas pipeline; hydrogen blending ratio; pipeline operational parameters



Academic Editor: Changmin Kim

Received: 18 November 2024

Revised: 8 December 2024

Accepted: 18 December 2024

Published: 27 December 2024

Citation: Li, J.-C.; Fan, Y.; Pang, D.; Wu, T.; Zhang, Y.; Zhou, K.

Investigation on the Compressibility Factor of Hydrogen-Doped Natural Gas Using GERG-2008 Equation of State. *Energies* **2025**, *18*, 53. <https://doi.org/10.3390/en18010053>

Copyright: © 2024 by the authors.

Licensee MDPI, Basel, Switzerland.

This article is an open access article distributed under the terms and conditions of the Creative Commons Attribution (CC BY) license (<https://creativecommons.org/licenses/by/4.0/>).

1. Introduction

Hydrogen, as an ideal energy carrier, is characterized by its high energy conversion efficiency and the fact that it only produces water vapor during use, without emitting greenhouse gases or other harmful pollutants, making it a zero-emission, abundantly renewable, highly efficient energy storage medium with high energy density, versatile applications, reduced dependency on fossil fuels, improved air quality, and the construction

of hybrid energy systems [1]. This makes it a promising option for achieving green, low-carbon development. In recent years, advancements in hydrogen production technology and the expansion of its application areas have propelled hydrogen into the spotlight within the energy sector. Notably, its use in transportation, industry, and construction is rapidly growing, demonstrating substantial commercial value and promising development prospects [2]. However, despite the strong momentum in the hydrogen industry, several key challenges must be addressed to enable large-scale adoption. First, low-cost, high-efficiency hydrogen production technology remains a primary barrier to widespread hydrogen use, especially regarding cost control for green hydrogen (hydrogen produced through water electrolysis). Additionally, breakthroughs in the safe storage and transportation of hydrogen are urgently needed to ensure a stable and reliable hydrogen supply chain.

In 1992, Lynch proposed the concept of transporting hydrogen-blended natural gas. This mixed delivery approach not only allows for the large-scale, long-distance, safe, and efficient transport of hydrogen, but also avoids the high costs associated with constructing dedicated hydrogen pipelines, making it an economically and technically feasible solution recognized internationally. Consequently, hydrogen-blended natural gas has garnered widespread attention as a novel energy carrier [3]. Zeng et al. used the Peng–Robinson equation of state to calculate the gas–liquid viscosity of hydrocarbons, finding that it demonstrated superior predictive accuracy compared to experimental values [4]. Ren et al. assessed the accuracy of the Sarem, CNGA, Peng–Robinson, AGA8-92DC, and BWRS equations of state in calculating the compression factor by comparing them to the Standing–Katz chart. They concluded that AGA8 and BWRS offered the highest accuracy, with deviations below 1%, followed by Sarem and PR, while CNGA showed the lowest accuracy [5]. Li et al. calculated the Joule–Thomson coefficient (JTC) for natural gas and hydrogen-blended natural gas under varying pressures (0.1–10 MPa) and temperatures (10–50 °C) using empirical formulas and the SRK, PR, and BWRS equations of state [6]. Pan et al. conducted numerical simulations of hydrogen-blended natural gas combustion, analyzing the effects of different hydrogen blending ratios on the flow field, temperature field, emission concentration, and overall pollutant emissions in gas turbine combustors. Their findings validated the engineering feasibility of hydrogen–methane blending [7]. Tong et al. investigated the outcomes of leakage and explosion incidents of hydrogen-blended natural gas under varying pipeline pressures and leakage directions, comparing peak explosion overpressures from different leak directions and their impact on buildings [8]. Wang et al. refined a non-adiabatic pipeline leakage model to study the flow characteristics of hydrogen-blended natural gas leakage. Their results indicated that increasing the initial pressure leads to a higher leakage rate and longer leakage duration, with lower temperatures observed at the same time points. Moreover, higher hydrogen concentrations resulted in slower mass leakage rates, greater pressure drop rates, and lower minimum temperatures [9]. Alaa et al. used the MLFN neural network to calculate the compressibility factor of natural gas, which facilitated the estimation of hydrocarbon content in natural gas based on its physical properties, proving that the MLFN neural network was an important, beneficial, and cost-effective technology for calculating the compressibility factor of natural gas [10].

Using existing pipelines to transport hydrogen-blended gas introduces new safety and technical challenges. Compared to methane, the primary component of natural gas, hydrogen has a smaller molecular size and behaves more like an ideal gas under equivalent pressure and temperature conditions, making it harder to compress. Consequently, when hydrogen is blended into natural gas pipelines, the compressibility factor of the transported medium changes, which in turn affects pipeline operating parameters, compressor characteristics, and other aspects of system performance [11]. The international standard ISO 20765-2 [12], published in 2015, employs the GERG-2008 equation of state to calculate

the thermophysical properties of natural gas across a wide range of temperatures and pressures [13]. Based on the GERG-2008 equation, it is possible to achieve more precise calculations of the compressibility factor for ultra-high-pressure natural gas. In this study, we developed a computational program for determining the compressibility factor based on ISO 20765-2 and the GERG-2008 equation of state and validated its accuracy.

In this study, we conducted experimental tests on the compressibility factor of a CH₄-H₂-N₂ ternary gas mixture across a temperature range of −10 °C to 110 °C and a pressure range of 2 to 12 MPa, with hydrogen blending ratios of 5%, 10%, 20%, 30%, and 40%. We analyzed how the compressibility factor of this ternary mixture varies with the hydrogen ratio, pressure, and temperature under these experimental conditions. The findings from this research provide valuable insights for optimizing and applying hydrogen-blended natural gas in transport channels, understanding combustion reactions, and adjusting pipeline operating parameters and compressor performance characteristics.

2. Compression Factor Calculation Method

2.1. Subsection AGA8-92DC Equation

The AGA8-92DC equation is primarily applied to pipeline gas transport within standard temperature and pressure ranges. Its fundamental form is as follows [5]:

$$Z = 1 + B\rho_m - \rho_r \sum_{n=13}^{18} C_n^* + \sum_{n=13}^{58} C_n^* \times (b_n - c_n k_n \rho_r^{k_n}) \rho_r^{b_n} \exp(-c_n \rho_r^{k_n}) \quad (1)$$

In this equation, B represents the second Virial coefficient; ρ_m is the molar density; ρ_r denotes the reduced density; b_n , c_n , and k_n are constants; and C_n^* is a coefficient that is a function of temperature and composition.

2.2. Regression Equation

The regression model is a mathematical fit of the Standing–Katz compressibility factor chart [14]. It includes various forms, such as cubic, exponential, explicit, and implicit equations, all using reduced pressure, reduced temperature, and relative density as input variables. For implicit equations, the Newton–Raphson method is used to obtain solutions.

2.2.1. Hall–Yarborough Equation

This method, developed by Hall and Yarborough, is derived from the Starling–Carnahan equation of state [15]. It is applicable within the range $0.1 \leq P_r \leq 15.0$ and $1.05 \leq T_r \leq 3.00$.

$$Z = \frac{0.06125T_r^{-1} \exp[-1.2(1 - T_r^{-1})^2]}{y} \quad (2)$$

2.2.2. Redlich–Kwong Equation

This method is derived from the Redlich–Kwong equation of state [16] and is a cubic equation in terms of the compressibility factor. It is applicable within the range $0.1 \leq P_r \leq 15.0$ and $1.05 \leq T_r \leq 3.00$.

$$Z^3 - Z^2 + Z(a^2 - b^2 p - b)p - a^2 b p^2 = 0 \quad (3)$$

$$a^2 = \frac{0.4278T_c^{2.5}}{p_c T^{2.5}} \quad (4)$$

$$b = \frac{0.0867T_c}{p_c T} \quad (5)$$

In this equation, p_c represents the critical pressure of natural gas (MPa), and T_c denotes the critical temperature of natural gas (K).

In 1972, Soave [17] proposed an improved version of the RK equation known as the Soave–Redlich–Kwong equation (abbreviated as the SRK equation):

$$Z^3 - Z^2 + (A - B - B^2)p - AB = 0 \quad (6)$$

$$A = \frac{ap}{(RT)^2} \quad (7)$$

$$B = \frac{bp}{RT} \quad (8)$$

In this equation, a and b are constants related to the types and states of the components in the mixture; p represents the absolute pressure (MPa); R is the universal gas constant J/(mol·K); and T denotes the temperature (K).

2.3. GERG-2008 Equation of State

The GERG-2008 equation of state was proposed by Kunz and Wagner in 2012 [12]. The equations required for calculating the compressibility factor are as follows:

$$Z = 1 + \delta\alpha_\delta^r \quad (9)$$

$$\delta = \frac{c}{(c_r(x))} \quad (10)$$

$$\tau = \frac{(T_r(x))}{T} \quad (11)$$

In this equation, Z represents the compressibility factor; α is the Helmholtz free energy; and α^r denotes the residual Helmholtz free energy. The subscripts δ and τ correspond to the reciprocal of the reduced density and reduced temperature, respectively, and are obtained using the following equation:

$c_r(x)$ and $T_r(x)$ are defined by Equations (4) and (5), where the subscript r denotes reduced conditions:

$$\frac{1}{(c_r(x))} = \sum_{i=1}^N \frac{x_i^2}{c_{c,i}} + \sum_{i=1}^{N-1} \sum_{j=i+1}^N 2x_i x_j \beta_{V,ij} \gamma_{V,ij} \times \frac{x_i + x_j}{\beta_{V,ij}^2 x_i + x_j} \frac{1}{8} \left(\frac{1}{c_{c,i}^{1/3}} + \frac{1}{c_{c,j}^{1/3}} \right)^3 \quad (12)$$

$$T_r(x) = \sum_{i=1}^N x_i^2 T_{c,i} + \sum_{i=1}^{N-1} \sum_{j=i+1}^N 2x_i x_j \beta_{T,ij} \gamma_{T,ij} \times \frac{x_i + x_j}{\beta_{T,ij}^2 x_i + x_j} (T_{c,i} T_{c,j})^{0.5} \quad (13)$$

In this equation, the subscripts i and j correspond to the respective components; c_c is the critical concentration mol/L; T_c represents the critical temperature; x_i and x_j denote the mole fractions of components i and j , respectively; and $\beta_{T,ij}$, $\gamma_{T,ij}$, $\beta_{V,ij}$, and $\gamma_{V,ij}$ are the binary interaction parameters, the values of which can be found in ISO 20765-2:2015 [12].

$$\alpha_\delta^r = \left(\frac{\partial \alpha^r}{\partial \delta} \right)_{\tau,x} = \sum_{i=1}^{N-1} 2x_i \left(\frac{\partial \alpha_i^r}{\partial \delta} \right)_\tau + \sum_{i=1}^{N-1} \sum_{j=i+1}^N x_i x_j F_{ij} \left(\frac{\partial \alpha_{ij}^r}{\partial \delta} \right)_\tau \quad (14)$$

$$\delta \left(\frac{\partial \alpha_i^r}{\partial \delta} \right)_\tau = \sum_{k=1}^{k_1} d_{i,k} n_{i,k} \delta^{d_{i,k}} \tau^{t_{i,k}} + \sum_{k=k_2}^{k_3} (d_{i,k} - c_{i,k} \delta^{c_{i,k}}) n_{i,k} \delta^{d_{i,k}} \tau^{t_{i,k}} \exp(-\delta^{c_{i,k}}) \quad (15)$$

$$\delta \left(\frac{\partial \alpha_{ij}^r}{\partial \delta} \right) = \sum_{k=1}^{k_1} d_{ij,k} n_{ij,k} \delta^{d_{ij,k}} \tau^{t_{ij,k}} + \sum_{k=k_2}^{k_3} n_{ij,k} \delta^{d_{ij,k}} \tau^{t_{ij,k}} \left[d_{ij,k} - 2\eta_{ij,k} \delta (\delta - \varepsilon_{ij,k}) - \delta \beta_{ij,k} \right] \times \exp \left[-\eta_{ij,k} (\delta - \varepsilon_{ij,k})^2 - \beta_{ij,k} (\delta - \gamma_{ij,k}) \right] \quad (16)$$

In this equation, $n_{i,k}$, $c_{i,k}$, $d_{i,k}$, and $t_{i,k}$ are coefficients and exponents; $d_{ij,k}$, $t_{ij,k}$, $n_{ij,k}$, $\eta_{ij,k}$, $\varepsilon_{ij,k}$, $\beta_{ij,k}$, and $\gamma_{ij,k}$ are the coefficients and exponents of the deviation function; and F_{ij} represents the binary interaction coefficient. Here, i and j range from 1 to 21, and the values of the coefficients and exponents can be found in ISO 20765-2:2015 [12].

From the analysis of Equations (9)–(16), it can be observed that there is only one unknown variable, the concentration ccc , in the process of solving for the compressibility factor. Therefore, the process of determining the compressibility factor can be regarded as solving a first-order nonlinear equation. Among the methods commonly used for solving first-order nonlinear equations are the Newton–Raphson method, the secant method, and the bisection method. In this study, the bisection method is employed to solve the compressibility factor of the CERG-2008 equation of state.

3. Results and Analysis

Through experimentation, this study investigated the compressibility factors of CH₄-H₂ impurity gas mixtures under five different hydrogen blending ratios of 5%, 10%, 20%, 30%, and 40%. The specific proportions of each gas are detailed in Table 1.

Figures 1–5 demonstrated the changes in the compressibility factor under different hydrogen blending ratios, temperatures, and pressures. These charts were used to visually display the impact of hydrogen blending on the compressibility factor of natural gas mixtures. This helped researchers understand how hydrogen doping affected the physical properties of natural gas, especially in actual pipeline transportation, where these properties significantly impact the fluidity and compressibility of the gas.

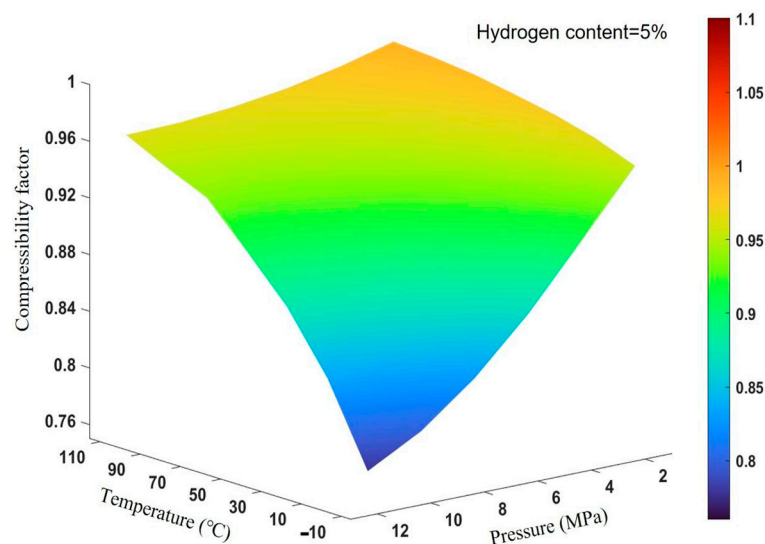


Figure 1. Compressibility factor of Case 1.

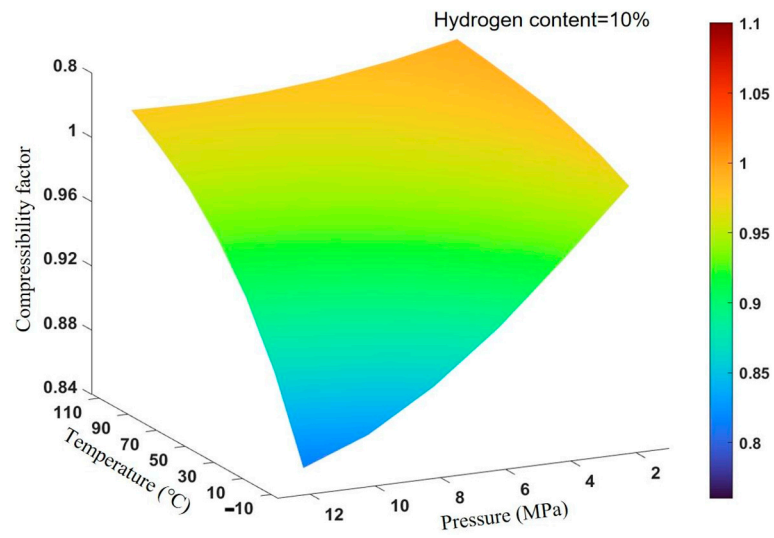


Figure 2. Compressibility factor of Case 2.

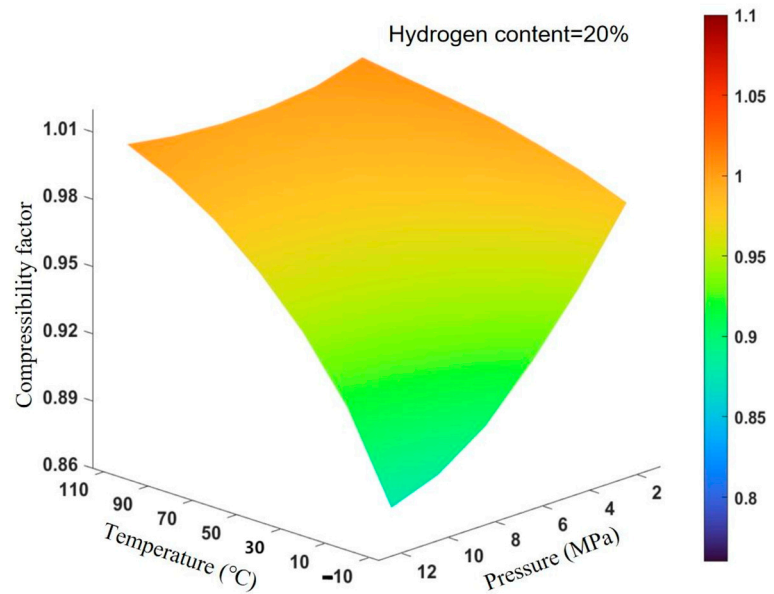


Figure 3. Compressibility factor of Case 3.

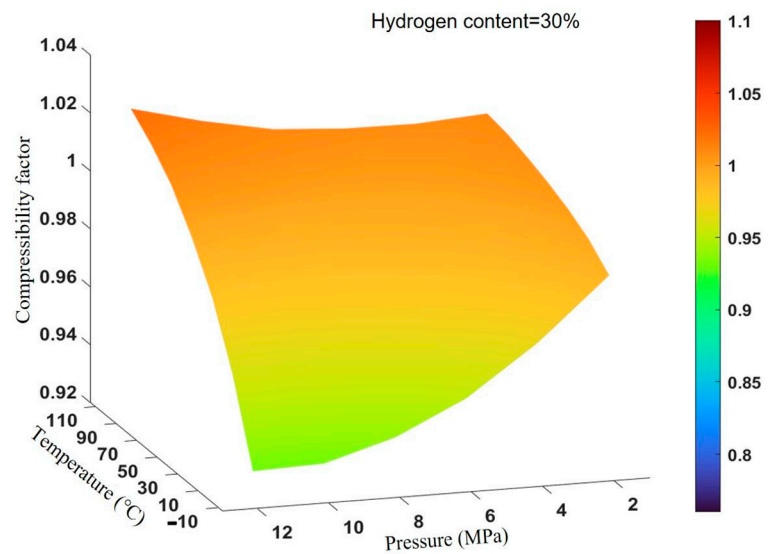


Figure 4. Compressibility factor of Case 4.

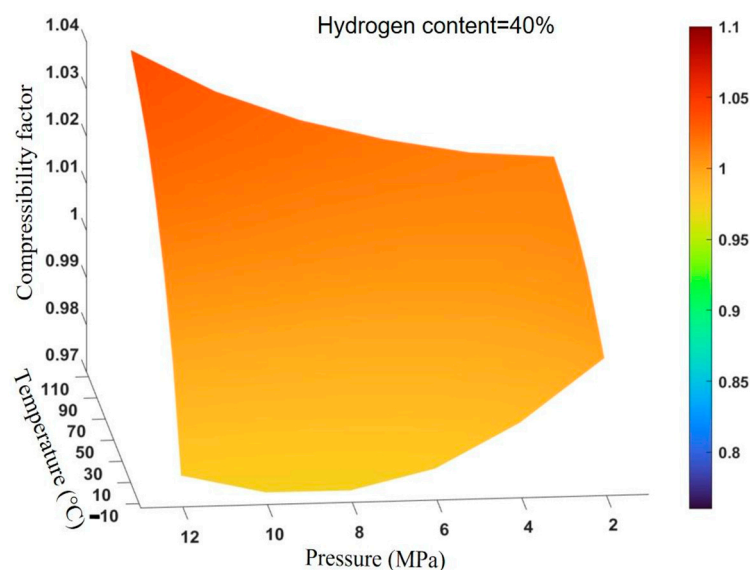


Figure 5. Compressibility factor of Case 5.

Table 1. Gas ratios under different working conditions.

Experimental Conditions	CH ₄	H ₂	Impurity Gas
Case 1	85.0%	5.0%	10.0%
Case 2	80.0%	10.0%	10.0%
Case 3	70.0%	20.0%	10.0%
Case 4	65.0%	30.0%	5.0%
Case 5	55.0%	40.0%	5.0%

3.1. Effect of Hydrogen Doping Ratio and Temperature

According to Figures 1–5, the compressibility factor of the mixed natural gas varies with the hydrogen blending ratio and temperature under the same pressure conditions. It can be concluded that, under these five experimental conditions, the compressibility factor ranges from 0.76 to 1.10. The minimum compressibility factor of 0.7781 occurs when the hydrogen content is 5%, with the temperature and pressure set at $-10\text{ }^{\circ}\text{C}$ and 12 MPa, respectively. Conversely, the maximum compressibility factor of 1.0390 is observed at a hydrogen content of 40%, with the temperature and pressure at $110\text{ }^{\circ}\text{C}$ and 12 MPa, respectively.

As the hydrogen blending ratio increases, there is a discernible upward trend in the compressibility factor. At lower temperatures (such as $-10\text{ }^{\circ}\text{C}$), the increase in the compressibility factor is particularly pronounced when the hydrogen blending ratio rises from 5% to 40%. For example, at a pressure of 10 MPa and a temperature of $-10\text{ }^{\circ}\text{C}$, the compressibility factor increases from 0.7986 to 0.9716 as the hydrogen ratio increases from 5% to 40%, corresponding to an approximate increase of 21.66%. Hydrogen, being the lightest element with a molecular weight of only 2 g/mol, lowers the average molecular weight of the mixture when blended with natural gas. This reduction in average molecular weight enhances the gas's compressibility, thereby increasing the compressibility factor. Additionally, the incorporation of hydrogen may alter the intermolecular forces within the gas mixture; due to the relatively weak intermolecular forces among hydrogen molecules, this could further contribute to increased compressibility. This trend is also observed at higher temperatures (such as $70\text{ }^{\circ}\text{C}$ and $90\text{ }^{\circ}\text{C}$), although the increase is relatively modest. This is attributed to the fact that rising temperatures elevate the average kinetic energy of gas molecules, thereby increasing the average distance between them and reducing the gas's compressibility. For instance, at a pressure of 10 MPa and a temperature of $110\text{ }^{\circ}\text{C}$,

the compressibility factor increases from 0.9637 to 1.0297 as the hydrogen blending ratio rises from 5% to 40%, resulting in an approximate increase of 6.85%.

Under the same pressure conditions, higher temperatures are associated with smaller variations in the growth rate of the compressibility factor, resulting in a slower increase in the compressibility factor from experimental condition 1 to experimental condition 5. Furthermore, an increase in pressure typically leads to a rise in the compressibility factor of the gas. As illustrated in Figures 1–5, when the hydrogen blending ratio and pressure are held constant, the compressibility factor tends to increase with rising temperature. For instance, at a hydrogen blending ratio of 40% and a pressure of 4 MPa, as the temperature increases from $-10\text{ }^{\circ}\text{C}$ to $110\text{ }^{\circ}\text{C}$, the compressibility factor rises from 0.9848 to 1.0152, reflecting an approximate increase of 3.09%. This phenomenon can be attributed to the lower average kinetic energy of gas molecules at low temperatures, which results in fewer molecular collisions.

Based on the analysis above, we can conclude that the gas volume responds more sensitively to changes in pressure, which makes the impact of increasing the hydrogen blending ratio on the compressibility factor more pronounced. In contrast, at higher temperatures, the average kinetic energy of gas molecules increases, leading to more frequent collisions. This results in an expansion of the gas volume, which in turn lowers the compressibility factor. This indicates that the impact of the hydrogen blending ratio on the compressibility factor is more pronounced under low-temperature conditions.

3.2. Effect of Hydrogen Doping Ratio and Pressure

As shown in Figures 1–5, at higher pressures (such as 10 MPa and 12 MPa), the increase in the compressibility factor is particularly pronounced when the hydrogen blending ratio rises from 5% to 40%. This phenomenon is attributed to the fact that higher temperatures increase the average kinetic energy of gas molecules, which in turn increases the average distance between molecules, thereby reducing the gas's compressibility. For example, at a pressure of 12 MPa and a temperature of $90\text{ }^{\circ}\text{C}$, the compressibility factor increases from 0.9637 to 1.0297 as the hydrogen blending ratio increases from 5% to 40%, corresponding to an approximate increase of 6.85%. This trend is also observed at lower pressures (such as 2 MPa), although the increase is relatively modest. For instance, at a pressure of 2 MPa and a temperature of $10\text{ }^{\circ}\text{C}$, as the hydrogen blending ratio increases from 5% to 40%, the compressibility factor rises from 0.9548 to 0.9980, reflecting an approximate increase of 4.52%.

The impact of pressure on the compressibility factor is also significant. At the same temperature, higher pressure results in larger variations in the growth rate of the compressibility factor, leading to a more rapid increase from experimental condition 1 to experimental condition 5. Moreover, increasing the temperature generally causes a decrease in the growth rate of the gas's compressibility factor. At lower pressures (such as 2 MPa), the values of the compressibility factor are relatively low, and the increase in the compressibility factor with rising hydrogen blending ratios is modest, with increments of 2.62%, 2.67%, 2.98%, 3.31%, 3.72%, 4.23%, and 5.07%. In contrast, at higher pressures (such as 12 MPa), the compressibility factor values are higher, and the increments associated with increasing hydrogen blending ratios are substantial, recorded as 9.21%, 10.58%, 11.70%, 14.78%, 17.92%, 22.81%, and 30.16%.

Based on the experimental analysis above, it is known that the effect of the hydrogen blending ratio on the compressibility factor is more significant. In high-pressure experimental environments, the distance between molecules decreases, leading to more pronounced intermolecular interactions, which in turn increases the non-ideality of the gas. Conversely,

in low-pressure experimental environments, the greater the distance between molecules, the weaker the interactions, causing the gas behavior to be closer to that of an ideal gas.

4. Conclusions

This study, based on the GERG-2008 equation of state, calculated the compressibility factors under various conditions. The experimental results revealed the variations in compressibility factors with respect to different temperatures, pressures, and hydrogen blending ratios. The main conclusions of this research are as follows:

- (1) At the same pressure, higher temperatures are associated with smaller variations in growth rates, resulting in a slower increase in the compressibility factor as the hydrogen blending ratio rises from 5% to 40%. Additionally, increasing temperature typically leads to an increase in the gas's compressibility factor.
- (2) At the same temperature, higher pressures are linked to greater variations in growth rates, causing a more rapid increase in the compressibility factor as the hydrogen blending ratio changes from 5% to 40%. Furthermore, increasing pressure usually results in an increase in the gas's compressibility factor.
- (3) The effect of the hydrogen blending ratio on the compressibility factor is more pronounced under low-temperature, high-pressure conditions. When the temperature and pressure are set at $-10\text{ }^{\circ}\text{C}$ and 12 MPa, respectively, increasing the hydrogen blending ratio from 5% to 40% results in the compressibility factor rising from 0.7781 to 1.0128, corresponding to a growth rate of 30.16%.
- (4) At a hydrogen content of 40%, a temperature of $110\text{ }^{\circ}\text{C}$, and a pressure of 12 MPa, the compressibility factor is 1.0390, and the working conditions are optimal. This results in a relatively high energy density of the gas, which allows for a more efficient use of the pipeline capacity during transportation. The overall energy density of the gas increases, reducing the construction and maintenance costs of pipelines, and improving transportation efficiency.

Additionally, different concentrations of hydrogen have a significant impact on the embrittlement of iron, with higher concentrations of hydrogen more likely to cause hydrogen embrittlement in iron. At the same time, as the hydrogen pressure increases, the embrittling effect of hydrogen typically increases as well, but the results vary depending on the material. The increase in hydrogen pressure usually leads to a decrease in fracture toughness [18]. It is recommended that future research should further evaluate the performance of different pipeline materials in hydrogen mixed-gas transportation, especially their susceptibility to hydrogen embrittlement under varying temperatures and pressures. This will provide a more reliable theoretical foundation and practical guidance for the safe transportation of hydrogen, thereby promoting the widespread application and sustainable development of hydrogen energy.

Author Contributions: Conceptualization, J.-C.L. and K.Z.; methodology, T.W.; software, Y.Z.; validation, D.P.; formal analysis, Y.F.; investigation, Y.F.; resources, T.W.; data curation, K.Z.; writing—original draft preparation, T.W.; writing—review and editing, J.-C.L.; visualization, Y.Z.; supervision, D.P.; project administration, K.Z.; funding acquisition, J.-C.L. All authors have read and agreed to the published version of the manuscript.

Funding: This research was funded by the “Hundred Outstanding Talents” Support Program of Jining University, a provincial-level key project in the field of natural sciences, grant number 2023ZYRC23.

Data Availability Statement: The data that support the findings of this study are available within the article.

Acknowledgments: This research is also the result of receiving support for the 2024 provincial college student's innovation and entrepreneurship training program project (Project: Liquid circulation cooling system for hydrogen storage tank of hydrogen energy vehicle), and Ludong University college students innovation and entrepreneurship training program, China.

Conflicts of Interest: Author Dan Pang was employed by the Liaoshen Industry Group Corporation Limited. The remaining authors declare that the research was conducted in the absence of any commercial or financial relationships that could be construed as a potential conflict of interest.

References

1. Sadeq, A.M. *Hydrogen: The Carrier of Future Energy*; Amazon: Seattle, WA, USA, 2023. [CrossRef]
2. Hu, B.; Xu, P.Y.; Wang, L.P.; Xiang, D.C.; Jiang, F.H.; Cao, D.F.; Liu, K. Stability analysis and multi-objective optimization of methanol steam reforming for on-line hydrogen production. *Int. J. Hydrogen Energy* **2024**, *91*, 434–446. [CrossRef]
3. Lynch, F.E.; Marmaro, R.W. Special Purpose Blends of Hydrogen and Natural Gas. U.S. Patent 5139002, 18 August 1992.
4. Zeng, Q.; Wang, L. Application of Peng-Robinson equation of state for calculation of liquid and gas viscosities of hydrocarbons. *Comput. Appl. Chem.* **2005**, *22*, 1187.
5. Ren, H.Y.; Li, C.J.; Xie, G. Evaluation of State Equations of Natural Gas in Pipeline Transportation. *Adv. Mater. Res.* **2012**, *463*, 936–939. [CrossRef]
6. Li, J.; Su, Y.; Yu, B.; Wang, P.; Sun, D. Influences of hydrogen blending on the Joule–Thomson coefficient of natural gas. *ACS Omega* **2021**, *6*, 16722–16735. [CrossRef] [PubMed]
7. Pan, W.G.; Kang, L.W.; Chi, Z.W.; Wang, W.H.; Tang, C.W. Numerical study on effects of hydrogen doping of natural gas on the combustion characteristics in micro gas turbine combustor. *Appl. Therm. Eng.* **2024**, *255*, 123989. [CrossRef]
8. Tong, S.R.; Li, X.; Ding, H.R.; Shuai, J.; Mei, Y.; Chan, S.H. Large-scale transient simulation for consequence analysis of hydrogen-doped natural gas leakage and explosion accidents. *Int. J. Hydrogen Energy* **2024**, *54*, 864–877. [CrossRef]
9. Wang, L.; Chen, J.; Ma, T.X.; Ma, R.L.; Bao, Y.Y.; Fan, Z.Y. Numerical study of leakage characteristics of hydrogen-blended natural gas in buried pipelines. *Int. J. Hydrogen Energy* **2024**, *49*, 1166–1179. [CrossRef]
10. Ghanem, A.; Gouda, M.F.; Alharthy, R.D.; Desouky, S.M. Predicting the compressibility factor of natural gas by using statistical modeling and neural network. *Energies* **2022**, *15*, 1807. [CrossRef]
11. Zhang, B.; Xu, N.; Zhang, H.R.; Qiu, R.; Wei, X.M.; Wang, Z.; Liang, Y.T. Influence of hydrogen blending on the operation of natural gas pipeline network considering the compressor power optimization. *Appl. Energy* **2024**, *358*, 122594. [CrossRef]
12. ISO 20765-2:2015; Natural Gas—Calculation of Thermodynamic Properties. International Organization for Standardization: Geneva, Switzerland, 2015.
13. Kunz, O.; Wagner, W. The GERG-2008 wide-range equation of state for natural gases and other mixtures: An expansion of GERG-2004. *J. Chem. Eng. Data* **2012**, *57*, 3032–3091. [CrossRef]
14. Standing, M.B.; Katz, D. Density of natural gases. *Transactions of the American Institute of Mining, Metall. Pet. Eng.* **1942**, *146*, 140–149.
15. Hall, K.R.; Yarborough, L. A new equation of state for Z-factor calculations. *Oil Gas J.* **1973**, *71*, 82–92.
16. Redlich, O.; Kwong, J.N. On the thermodynamics of solutions. V. An equation of state. Fugacities of gaseous solutions. *Chem. Rev.* **1949**, *44*, 233–244. [CrossRef]
17. Soave, G. Equilibrium constants from a modified Redlich-Kwong equation of state. *Chem. Eng. Sci.* **1972**, *27*, 1197–1203. [CrossRef]
18. Barthélémy, H. Effects of pressure and purity on the hydrogen embrittlement of steels. *Int. J. Hydrogen Energy* **2011**, *36*, 2750–2758. [CrossRef]

Disclaimer/Publisher's Note: The statements, opinions and data contained in all publications are solely those of the individual author(s) and contributor(s) and not of MDPI and/or the editor(s). MDPI and/or the editor(s) disclaim responsibility for any injury to people or property resulting from any ideas, methods, instructions or products referred to in the content.